Interferon Regulatory Factor 4 Regulates Obesity-Induced Inflammation Through Regulation of Adipose Tissue Macrophage Polarization

Jun Eguchi,[1,2] Xingxing Kong,[1] Masafumi Tenta,[2] Xun Wang,[1] Sona Kang,[1] and Evan D. Rosen[1,3]

Interferon regulatory factors (IRFs) play functionally diverse roles in the transcriptional regulation of the immune system. We have previously shown that several IRFs are regulators of adipogenesis and that IRF4 is a critical transcriptional regulator of adipocyte lipid handling. However, the functional role of IRF4 in adipose tissue macrophages (ATMs) remains unclear, despite high expression there. Here we show that IRF4 expression is regulated in primary macrophages and in ATMs of high-fat diet–induced obese mice. *Irf4*$^{-/-}$ macrophages produce higher levels of proinflammatory cytokines, including interleukin-1β and tumor necrosis factor-α, in response to fatty acids. In coculture experiments, IRF4 deletion in macrophages leads to reduced insulin signaling and glucose uptake in 3T3-L1 adipocytes. To determine the macrophage-specific function of IRF4 in the context of obesity, we generated myeloid cell–specific IRF4 knockout mice, which develop significant insulin resistance on a high-fat diet, despite no difference in adiposity. This phenotype is associated with increased expression of inflammatory genes and decreased insulin signaling in adipose tissue, skeletal muscle, and liver. Furthermore, *Irf4*$^{-/-}$ ATMs express markers suggestive of enhanced M1 polarization. These findings indicate that IRF4 is a negative regulator of inflammation in diet-induced obesity, in part through regulation of macrophage polarization. ***Diabetes*** **62:3394–3403, 2013**

The last decade has seen a sharp increase in our appreciation for the macrophage as a critical regulator of metabolic status in obesity. Under high nutrient conditions, macrophages infiltrate peripheral tissues, where they elaborate cytokines that negatively affect insulin action. More recently, it has become clear macrophages are not uniform in their propensity to promote inflammation. Instead, macrophages exist on a continuum defined by those that secrete proinflammatory cytokines, such as tumor necrosis factor-α (TNF-α) and interleukin (IL)-1β (so-called M1 macrophages) on one end, and those that secrete anti-inflammatory cytokines, such as IL-10 (so-called M2 macrophages), on the other (1–3). M2 macrophages participate in tissue remodeling, protect against parasitic infections, and are overrepresented among macrophages that reside within adipose tissue normally (ATMs). During high-fat feeding, macrophages of both classes increase in abundance in adipose tissue; however, the increase is significantly greater for the M1 subclass (2,4–6). The consequences of this imbalance toward M1 recruitment into adipose tissue in obesity include insulin resistance and metabolic dysfunction (7).

The molecular pathways that promote macrophage polarization have been under intensive study. M1 macrophages are activated by γ-interferon and Toll-like receptor (TLR4) signaling through a variety of intermediates, including the transcription factors STAT1, nuclear factor (NF)-κB, and various members of the interferon regulatory factor (IRF) family such as IRF3 (2). The M2 phenotype, on the other hand, is induced by cytokines such as IL-4 and IL-13 and is promoted and maintained by the actions of transcription factors such as STAT6 (1), peroxisome proliferator–activated receptor γ (PPARγ) (8,9), PPARδ (10), and Kruppel-like factor 4 (KLF4) (11). Unique among the IRF family, the transcription factor IRF4 has also been associated with M2 polarization (12,13). IRF4 expression in macrophages was elevated in response to helminthic infection, and M2 marker genes were reduced in *Irf4*$^{-/-}$ bone marrow–derived macrophages (13). The microRNA miR-125b, which represses IRF4 expression, was recently shown to promote inflammatory activation of macrophages (14). Consistent with this in vitro observation, global *Irf4*$^{-/-}$ mice display enhanced systemic inflammation, although they are protected from lupus nephritis secondary to effects on B and T lymphocytes, two other cell types in which IRF4 plays an important functional role (15).

We identified IRF4 in an epigenomic screen for transcription factors that affect adipogenesis; IRF4 is expressed in a developmentally regulated manner in adipocytes and acts as a potent repressor of differentiation (16). We subsequently studied the effect of IRF4 in mature adipocytes, using a tissue-specific knockout model, and showed that IRF4 plays a critical role in adipose lipolysis and lipogenesis (17). Adipose-specific IRF4 knockout mice show increased weight gain on a high-fat diet and are subsequently more insulin resistant than their control littermates. We speculated that IRF4 might affect insulin sensitivity via actions in other cell types, particularly macrophages. Specifically, we hypothesized a role for IRF4 in suppressing M1 polarization and the subsequent release of cytokines that promote insulin resistance. Here, we show that IRF4 promotes M2 polarization of macrophages and is responsible for dampening the inflammatory response to palmitic acid and lipopolysaccharide (LPS). Furthermore, *Irf4*$^{-/-}$ macrophages induce insulin resistance in cocultured adipocytes, and mice with a macrophage-specific deletion of IRF4 display increased insulin resistance in the absence of changes in adiposity. Taken together with our

From the [1]Division of Endocrinology, Beth Israel Deaconess Medical Center, Boston, Massachusetts; the [2]Department of Medicine and Clinical Science, Okayama University Graduate School of Medicine and Dentistry, Okayama, Japan; and [3]Harvard Medical School, Boston, Massachusetts.
Corresponding author: Evan D. Rosen, erosen@bidmc.harvard.edu.
Received 26 September 2012 and accepted 26 June 2013.
DOI: 10.2337/db12-1327
This article contains Supplementary Data online at http://diabetes.diabetesjournals.org/lookup/suppl/doi:10.2337/db12-1327/-/DC1.
J.E. and X.K. contributed equally to this work.

prior results, IRF4 promotes insulin sensitivity through actions in at least two distinct tissues: adipocytes and macrophages.

RESEARCH DESIGN AND METHODS

Materials. Antibodies for Western blotting were purchased from Santa Cruz Biotechnology (IRF4, sc-6059), Cell Signaling Technology (Akt, 9272; p-Akt Ser473, 9271; JNK1, 3702; SAPK/JNK Kinase assay kit, 9810), and Millipore Inc. (IRS1 06-248; p-IRS1Ser307 07-247, Tubulin, MAB3408). The coding region of mouse IRF4 was isolated from 3T3-L1 adipocyte mRNA by RT-PCR using TaKaRa EX Taq polymerase (Takara Bio Inc.) and subcloned into pCDH-puro lentiviral vector (System Biosciences) for expression in mammalian cells.

Cell culture. 3T3-L1 cells (American Type Culture Collection) were cultured in Dulbecco's modified Eagle's medium (Invitrogen) with 10% bovine calf serum (Hyclone) in 5% CO_2. Two days after confluence, cells were exposed to Dulbecco's modified Eagle's medium/10% FBS (Invitrogen) with 1 μmol/L dexamethasone (Sigma), 5 μg/mL insulin (Sigma), and 0.5 mmol/L isobutyl methylxanthine (Sigma). After 2 days, cells were maintained in medium containing FBS only. RAW264.7 cells (American Type Culture Collection) were cultured in RPMI 1640 (Sigma) with 10% FBS (Invitrogen) in 5% CO_2. Peritoneal macrophages (PMs) from MI4KO and FLOX mice were isolated 4 days after intraperitoneal injection of 4% thioglycollate (BD Diagnostics), and resuspended in RPMI 1640 with 10% FBS. Cells were plated at a density of 2×10^5 cells per 1 well of a 24-well dish. Bone marrow–derived macrophages (BMDMs) were harvested from the femur and tibia, and then resuspended in RPMI 1640 with 10% FBS. The bone marrow cells were differentiated into M1 or M2 macrophages in RPMI 1640 with 10% FBS and 50 ng/mL granulocyte macrophage colony-stimulating factor (GM-CSF; Peprotech) or 50 ng/mL macrophage (M)-CSF (Peprotech) for 7 days. For stimulation experiments, PMs or BMDMs were incubated in serum-free RPMI 1640 containing 10 ng/mL LPS (Sigma), 10 ng/mL IL-4 (Miltenyi Biotec), or 200 μmol/L palmitate (Sigma). Palmitate-containing medium was prepared as previously described (18).

For time course experiments, BMDMs were incubated in serum-free RPMI 1640 containing 10 ng/mL LPS. Total RNA was harvested 0–8 h after LPS stimulation, and expression levels of target genes were measured by quantitative PCR (QPCR).

Coculture experiments. Coculture of 3T3-L1 adipocytes and PMs was performed as described previously (19,20). In the direct coculture experiments, 3T3-L1 adipocytes were cultured in a 12-well plate, and PMs were then plated directly into the same wells. Cells were cultured overnight before glucose uptake assay or insulin signaling study. In the indirect coculture experiments, 3T3-L1 adipocytes were differentiated in 12-well plates and then treated with conditioned medium from LPS-activated wild-type (WT) or *Irf4*$^{-/-}$ macrophages. Cells were cultured overnight before glucose uptake assay or insulin signaling study.

ELISA measurement of TNF-α. Serum levels of TNF-α from PMs were measured by ELISA (Biolegend).

Cell migration assay. Chemotaxis assay of BMDMs was performed using the QCM Cell Migration Assay kit (Millipore). BMDMs were placed in the upper compartment and subsequently incubated at 37°C. After 1 h, 100 ng/mL monocyte chemoattractant protein-1 (Peprotech) or conditioned medium from 3T3-L1 adipocytes was added to IMDM/0.5% FCS in the lower compartment. Control assays were performed without chemokine. After incubation for 4 h, transmigrated cells were stained with DAPI, and nuclei were counted under a fluorescence microscope.

Animals. Primary macrophage studies were performed using C57BL/6J mice obtained from The Jackson Laboratory and fed a standard diet (8664, Harlan Teklad). Mice were maintained under a 14-h light/10-h dark cycle at constant temperature (22°C) with free access to food and water. All animal studies were approved by the Beth Israel Deaconess Medical Center Institutional Animal Care and Use Committee. For DIO mice, C57BL/6J mice were fed a high-fat diet (D12331; Research Diets Inc.) for 12 weeks. Body weight was measured weekly. Magnetic resonance imaging (MRI; Echo Medical Systems) was used to examine body composition of mice.

Generation of MI4KO mice. *Irf4*$^{flox/flox}$ mice were generated as described previously (21). LysM-Cre mice were purchased from The Jackson Laboratory and mated with *Irf4*$^{flox/flox}$ mice, and cohorts were established by mating F1 *Irf4*$^{flox/+}$; *Cre*$^{+}$ mice to littermate *Irf4*$^{flox/+}$; *Cre*$^{-}$ mice. Mice were maintained under a 14-h light/10-h dark cycle at constant temperature (22°C) with free access to food and water and were fed a standard chow diet (8664, Harlan Teklad) or a high-fat diet (D12331; Research Diets Inc.).

Glucose, insulin, and pyruvate tolerance tests. For the glucose tolerance test (GTT), mice were fasted for 12 h and then injected subcutaneously with glucose (1.0 g/kg body weight). Blood samples were taken at regular time points (0–120 min), and blood glucose levels were determined with a portable glucose meter. For insulin tolerance tests, mice were fasted for 4 h and handled 30 min before being injected subcutaneously with human regular insulin (2.0 units/kg body weight). Blood samples were taken at regular intervals (0–120 min), and blood glucose was measured as described above. For pyruvate tolerance tests, mice were fasted overnight before intraperitoneal pyruvate administration (2 g/kg).

Insulin measurement. Serum was obtained from overnight-fasted mice or from animals receiving a GTT, and insulin levels were quantified using ELISA (Chrystal Chem) according to the manufacturer's protocol.

Insulin signaling studies. For in vivo insulin signaling, mice were fasted overnight and injected intraperitoneally with insulin (10 units/kg). Animals were killed 7 min after insulin injections. Their tissues were harvested immediately and subjected to Western blot analysis. For in vitro insulin signaling, 3T3-L1 adipocytes were serum-starved and stimulated with 100 nmol/L insulin for 15 min. Cell lysates were then subjected to Western blotting. All blots were quantified using ImageJ software (National Institutes of Health, Bethesda, MD).

Protein extraction and Western blot analysis. Tissue and cell lysates were prepared using radioimmunoprecipitation assay buffer (Boston BioProducts) supplemented with complete protease inhibitor cocktail (Roche). For Western blot analyses, 50 μg protein was subjected to SDS-PAGE under reducing conditions, transferred, and blotted using specific antibodies described above.

Histology and immunohistochemistry. Epididymal adipose tissue was fixed for 12–16 h at room temperature and embedded in paraffin. Hematoxylin and eosin (H&E) staining was performed. To detect macrophages in adipose sections, immunohistochemistry was performed using an antibody against the macrophage marker F4/80 (Abcam). Four mice for each genotype were used, and for each adipose depot, four fields per section were analyzed. The percentage of F4/80-positive cells was calculated as the number of nuclei of F4/80-positive cells divided by the total number of nuclei present in a field.

Glucose uptake assay. Cells in 12-well plates were washed twice with Krebs-Ringer (KR) phosphate buffer (127 mmol/L NaCl, 4.7 mmol/L KCl, 0.9 mmol/L $MgSO_4$, 10 mmol/L $NaPO_4$, 0.9 mmol/L $CaCl_2$) and incubated with prewarmed KR phosphate buffer containing 0.2% fatty acid–free BSA and 100 nmol/L insulin. The dish was then allowed to float in a 37°C water bath for 30 min. After this period, ^{3}H-2-deoxyglucose and unlabeled ^{3}H-2-deoxyglucose were dispensed into each well for a final concentration of 1 uCi/mL and 0.1 mmol/L, respectively. Cells were incubated for an additional 5 min at 37°C, and the reaction was stopped by adding ice-cold PBS. Lysis buffer was applied to each well. After 10 min at room temperature, each well was counted in a scintillation counter.

Analysis of gene expression by QPCR. Total RNA was extracted from cells or tissues using TRIzol reagent (Invitrogen), following the manufacturer's instructions. First-strand cDNA synthesis was performed using RETROscript (Ambion). Total RNA was converted into first-strand cDNA using oligo(dT) primers as described by the manufacturer. PCR was performed using cDNA synthesized from 1 μg total RNA in an Mx3000P QPCR system (Stratagene) with specific primers and SYBR Green PCR Master Mix (Stratagene). The relative abundance of mRNAs was standardized using *36B4* mRNA or *Gapdh* mRNA as the invariant control. Primers used are listed in the Supplemental Table 1.

Luciferase reporter assay. pNF-κB-Luc vectors were purchased from Clontech (631743). PMs were detached with trypsin and transfected using the Amaxa nucleofection system (Amaxa Biosystems). Transfections were performed using reporter construct (2 μg) along with galactosidase expression vector (100 ng) a transfection control. Luciferase activity was measured 16 h after transfection using the Galacto-Star luciferase reporter assay (Roche), according to the manufacturer's instructions.

Stromal-vascular fraction isolation. Stromal-vascular fraction (SVF) cells were isolated from epididymal fat depots in KR HEPES buffer by collagenase digestion as described (22).

ATM purification by flow cytometry and cell sorting. SVF pellets were resuspended in RBC Lysis Buffer (eBioscience) and incubated for 5 min before resuspension in sorting buffer (PBS with 0.5% endotoxin-free FBS, 2 mmol/L EDTA, and 25 mmol/L HEPES). Cells were incubated with Fc Block (BD Biosciences) before staining with conjugated antibodies for 15 min at 4°C, followed by two washes in 10× excess sorting buffer. Cells were resuspended in sorting buffer supplemented with DAPI and then analyzed by FACSAria (BD Biosciences). Viable cells were sorted directly into RNA lysis buffer for RNA extraction. ATMs were identified by coexpression of F4/80 and CD11b. Alexa Fluor 647-conjugated anti-CD206 was purchased from AbD Serotec. PE-conjugated anti-CD11c and anti-CD11b, PE/Cy5-conjugated anti-F4/80, allophycocyanin-conjugated anti-CD11c, and isotype antibodies were purchased from eBioscience.

Statistical analysis. Unpaired two-tailed Student *t* tests and two-way ANOVA were used. $P < 0.05$ was considered statistically significant.

RESULTS

IRF4 gene expression is induced by fatty acids and IL-4 in macrophages. LPS-dependent activation of TLR4 signaling induces the expression of inflammatory cytokines, such as IL-1β and TNF-α in macrophages, whereas IL-4 treatment induces an alternative state of macrophage activation (2,23). Using two macrophage models, thioglycollate-elicited mouse PMs and M-CSF–differentiated mouse BMDMs, we confirmed that TLR4 stimulation using LPS or the fatty acid palmitate induced expression of *Il1b* and *Tnfa*, whereas IL-4 stimulation repressed these genes (Fig. 1*A*). Conversely, markers of M2 macrophage polarization, such as *Arg1* and *Chi3l3*, were induced by IL-4 and repressed by TLR4 activation (Fig. 1*B*). IRF4 has been shown to promote M2 polarization of macrophages; as such, the pronounced induction of *Irf4* expression in macrophages by IL-4 was unsurprising (Fig. 1*C*). Somewhat paradoxically, previous reports that LPS can also activate *Irf4* expression were confirmed. Furthermore, activation of TLR4 by palmitate had the same effect, although induction by IL-4 was significantly more robust than by either TLR4 ligand.

IRF4 deficiency enhances proinflammatory cytokine production in macrophages in response to palmitate. Given that IRF4 plays an anti-inflammatory role in macrophages (24,25), its induction by TLR4 signaling suggests

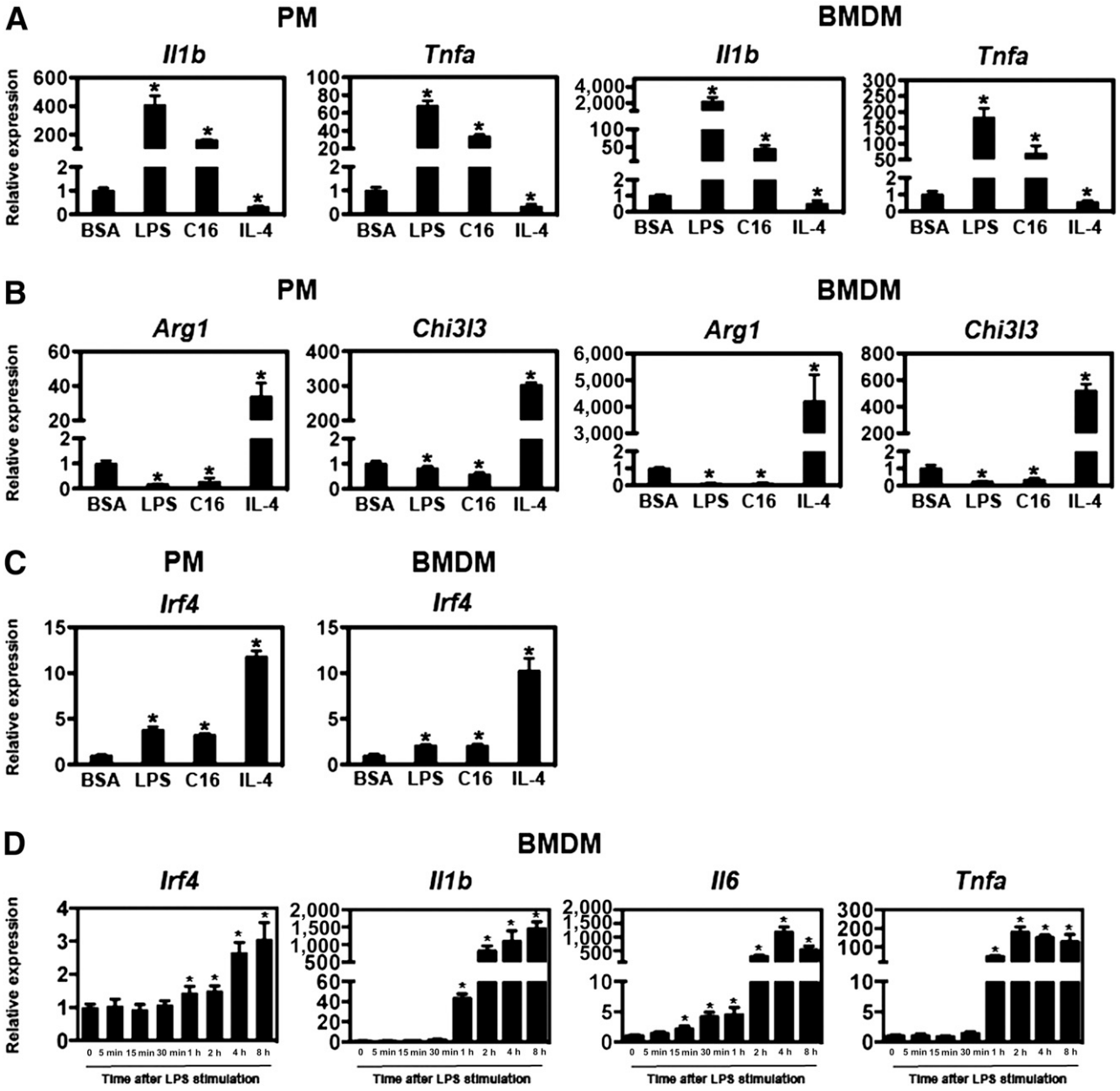

FIG. 1. TLR4 activation and IL-4 both induce IRF4 expression in macrophages. *A*: Expression of *Il1b* and *Tnfa* is induced by LPS and palmitate and repressed by IL-4 in activated PMs and BMDMs. *B*: Expression of *Arg1* and *Chi3l3* is repressed by LPS and palmitate and induced by IL-4 in activated primary PMs and BMDMs. *C*: Expression of *Irf4* is induced by LPS, palmitate, and IL-4 in activated primary PMs and BMDMs. *D*: Expression of *Irf4* peaks after the rise in inflammatory gene expression in response to LPS in BMDMs. *A–C*: RNA was harvested 16 h after treatment with LPS (10 ng/mL), palmitate (C16; 200 μmol/L), and IL-4 (10 ng/mL). *D*: Treatment with LPS was carried out for the indicated times. Data are normalized to *Gapdh* expression and are expressed as fold induction relative to BSA control. Results expressed as mean ± SD ($n = 5$). *$P < 0.05$.

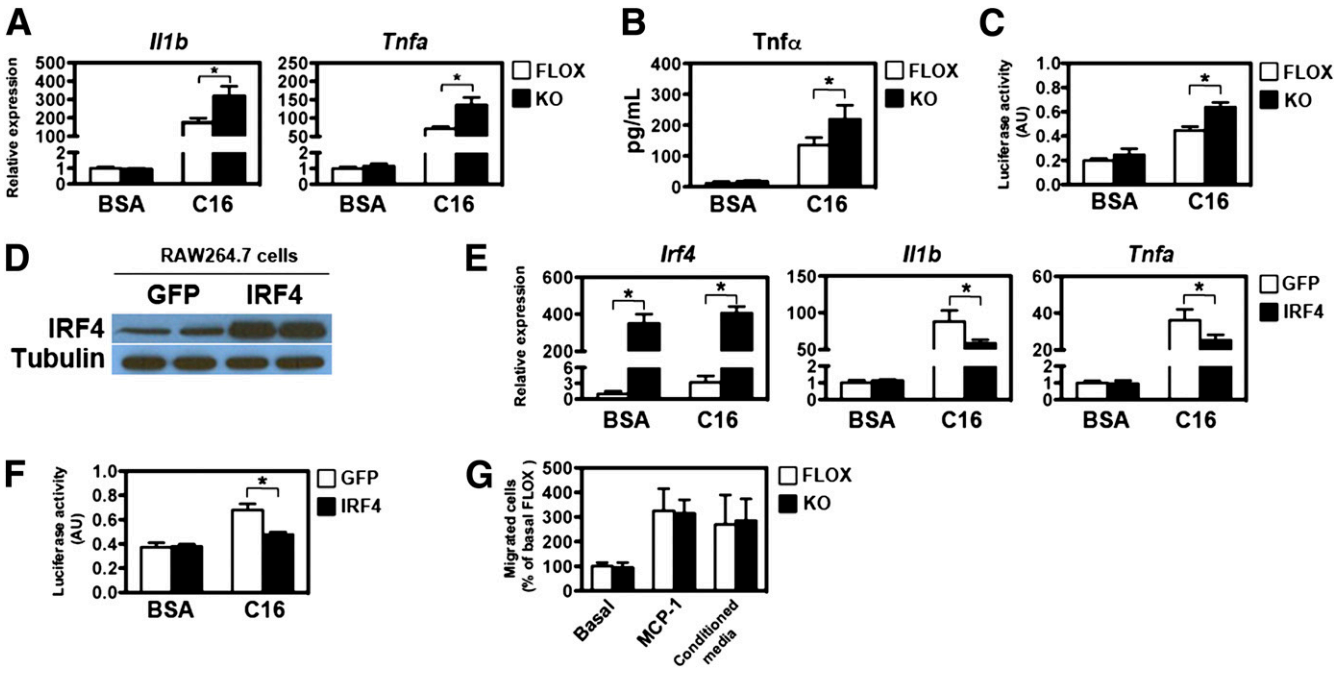

FIG. 2. Hyper-responsiveness of *Irf4*$^{-/-}$ macrophages to C16 stimulation in vitro. *A*: mRNA expression of *Il1b* and *Tnfa* in control (*Irf4*$^{flox/flox}$: FLOX) and *Irf4*$^{-/-}$ (KO) PMs. QPCR analysis of *Il1b* and *Tnfa* levels after 16-h stimulation with BSA or 200 μmol/L palmitate (C16). Data are normalized to *Gapdh* expression and are expressed as fold induction relative to BSA. Results expressed as mean ± SD (n = 5). *P < 0.05. *B*: Supernatant from FLOX and IRF4 KO PMs was collected 16 h after palmitate stimulation, and TNF-α levels were measured by ELISA. Results expressed as mean ± SD. *P < 0.05. *C*: Quantification of NF-κB promoter activity in PMs transfected with pNF-κB-Luc reporter plasmids after 16-h treatment with BSA or 200 μmol/L palmitate (C16). Data are normalized to β-gal expression. Results expressed as mean ± SD (n = 5). *P < 0.05. *D*: Western blot of RAW264.7 cells after transduction with lentivirus expressing green fluorescent protein (GFP) or IRF4. *E*: mRNA expression of *Irf4*, *Il1b*, and *Tnfa* in RAW264.7 cells expressing GFP or IRF4. QPCR analysis of *Irf4*, *Il1b*, and *Tnfa* after 16-h stimulation with BSA or 200 μmol/L palmitate (C16). Data are normalized to *Gapdh* expression and expressed as fold induction relative to BSA. Results expressed as mean ± SD (n = 5). *P < 0.05. *F*: Quantification of NF-κB promoter activity in RAW264.7 cells expressing GFP or IRF4 and transfected with pNF-κB-Luc reporter plasmids after 16-h treatment with BSA or 200 μmol/L palmitate (C16). Data are normalized to β-gal expression. Results expressed as mean ± SD (n = 5). *P < 0.05. *G*: Chemotaxis of FLOX and *Irf4* KO BMDMs was analyzed using a transwell migration assay. Results expressed as mean ± SD (n = 6) from three independent experiments. AU, arbitrary unit.

a compensatory or "braking" function. This is consistent with detailed time course data, which demonstrate that LPS-induced inflammatory gene expression peaks before *Irf4* (Fig. 1*D*). To assess this in the context of palmitate stimulation, we performed loss- and gain-of-function experiments. First, we isolated WT and IRF4 knockout (*Irf4*$^{-/-}$) PMs and treated these cells with palmitate. *Irf4*$^{-/-}$ PMs produced higher levels of proinflammatory cytokines, such as IL-1β and TNF-α, in response to palmitate than WT PMs (Fig. 2*A* and *B*). NF-κB is a critical downstream transcription factor in cytokine production in macrophages (18,26,27). WT and *Irf4*$^{-/-}$ PMs were transiently transfected with an NF-κB luciferase reporter construct, and then treated with 200 μmol/L palmitate. Palmitate significantly increased NF-κB transcriptional activity in *Irf4*$^{-/-}$ PMs to a greater degree than in WT cells (Fig. 2*C*). For gain-of-function studies, we transduced an IRF4 expression construct into the macrophage cell line RAW264.7 and then treated the cells with palmitate and examined cytokine expression. Overexpression of IRF4 (Fig. 2*D*) significantly blocked fatty acid–induced cytokine expression, and this was also associated with reduced NF-κB transcriptional activity (Fig. 2*E* and *F*). These data indicate that IRF4 is a negative regulator of fatty acid–induced production of inflammatory cytokines in macrophages. Loss of IRF4 did not affect all macrophage functions, however, because chemotaxis was unaffected in the presence of 100 ng/mL monocyte chemoattractant protein-1 or conditioned medium from differentiated 3T3-L1 adipocytes (Fig. 2*G*).

IRF4 deficiency in macrophages induces insulin resistance in cocultured adipocytes in vitro. If loss of IRF4 promotes a proinflammatory state in macrophages, that would be predicted to have an adverse effect on the insulin sensitivity of nearby adipocytes. To evaluate the effect of macrophage IRF4 on paracrine interactions with adipocytes, we performed two different types of coculture experiment. The first was a direct coculture assay, in which WT or *Irf4*$^{-/-}$ PMs were plated alongside differentiated 3T3-L1 adipocytes in the same dish before assessment of insulin-stimulated glucose uptake. In this model, activation of macrophages occurs through release of fatty acids from the adipocytes in coculture. Relative to WT macrophages, adipocytes in direct contact with *Irf4*$^{-/-}$ macrophages showed markedly reduced insulin-stimulated glucose uptake (Fig. 3*A*). We next performed an indirect coculture experiment in which we added conditioned medium from LPS-activated WT or *Irf4*$^{-/-}$ macrophages to mature 3T3-L1 adipocytes. Again, exposure to conditioned medium from *Irf4*$^{-/-}$ macrophages reduced insulin-stimulated glucose uptake compared with conditioned medium from WT macrophages (Fig. 3*B*). Moreover, add-back of IRF4 to *Irf4*$^{-/-}$ macrophages was able to fully revert adipocyte insulin responsiveness in the direct coculture assay (Fig. 3*C*). These changes in glucose uptake were mirrored by changes in insulin signaling, with *Irf4*$^{-/-}$ macrophages repressing insulin-stimulated IRS-1 and Akt2 phosphorylation in cocultured adipocytes (Fig. 3*D*). Forced expression of IRF4 in *Irf4*$^{-/-}$ macrophages restored these

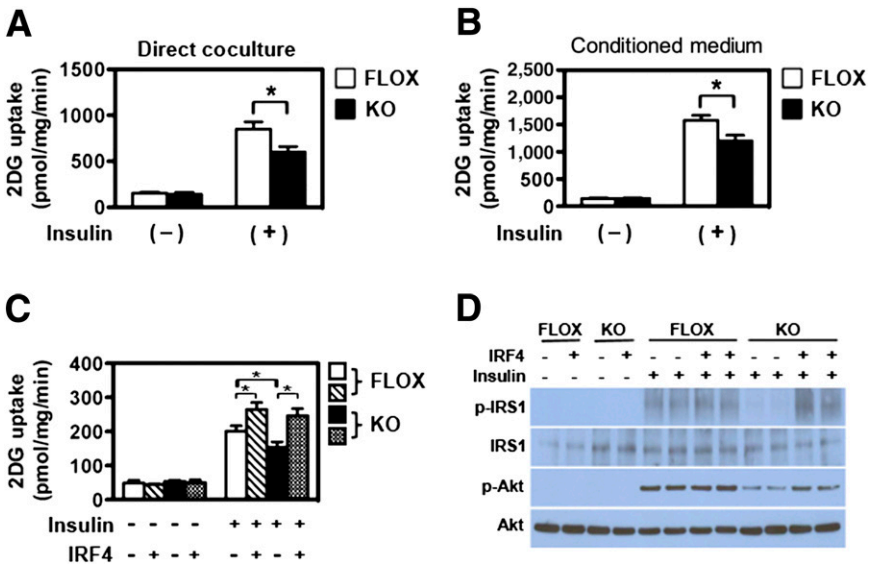

FIG. 3. IRF4 deficiency in macrophages induces insulin resistance in cocultured adipocytes in control ($Irf4^{flox/flox}$; FLOX) or $Irf4^{-/-}$ (KO) mice. *A*: Insulin (100 nmol/L) stimulation of ^{3}H-2-deoxyglucose (2DG) uptake was determined in 3T3-L1 adipocytes incubated in direct contact with FLOX or KO PMs. Results expressed as mean ± SD (n = 6) from three independent experiments. *P < 0.05. *B*: Insulin (100 nmol/L) stimulation of 2DG uptake was determined in 3T3-L1 adipocytes incubated with conditioned medium from FLOX or KO PMs. Results expressed as mean ± SD (n = 6) from three independent experiments. *P < 0.05. *C*: Insulin (100 nmol/L) stimulation of 2DG uptake was determined in 3T3-L1 adipocytes incubated in contact with FLOX or KO PMs, with and without the addition of exogenous IRF4. Results expressed as mean ± SD (n = 6) from three independent experiments. *P < 0.05. *D*: Insulin-stimulated phosphorylation of IRS1 and Akt in 3T3-L1 adipocytes incubated in direct contact with FLOX or KO PMs, with and without the addition of exogenous IRF4.

signaling events. Interestingly, overexpression of IRF4 in WT macrophages further enhanced insulin action in cocultured adipocytes (Fig. 3*C*) but did not demonstrably alter these signaling pathways (Fig. 3*D*), suggesting additional IRF4-dependent events that may lie further downstream in the insulin signaling cascade leading to glucose uptake.

Myeloid cell–specific deletion of IRF4 results in enhanced systemic insulin resistance. We sought next to extend our in vitro findings to a more physiologically relevant system. IRF4 was originally reported as a lymphocyte-specific transcriptional factor, although we now realize that it is highly expressed in macrophages and adipocytes as well (16,28,29). Because we wished to avoid confounding effects in lymphocytes, however, we crossed $Irf4^{flox/flox}$ mice with mice expressing Cre recombinase in a myeloid cell–specific manner (LysM-Cre), thus generating myeloid cell-specific IRF4 knockout mice (hereafter referred to as MI4KO). MI4KO mice showed virtually complete absence of IRF4 mRNA and protein in macrophages (Fig. 4*A* and *B*), without affecting the expression of IRF4 in B lymphocytes, T lymphocytes, or adipocytes (Fig. 4*A*). MI4KO mice were born in a Mendelian ratio, and there were no obvious morphological differences from control mice (WT, Cre only, or $Irf4^{flox/flox}$) in young animals (data not shown).

Total body weight of MI4KO mice was not different from controls, and MRI detected no significant changes in fat or lean mass on the chow or high-fat diet (Fig. 4*C–F*). Glucose tolerance and insulin sensitivity were similar in MI4KO and control mice fed a chow diet (Fig. 4*G* and *H*). On the high-fat diet, however, MI4KO mice demonstrated significantly impaired insulin tolerance and mildly reduced glucose tolerance overall, with a nonsignificant trend toward elevated evoked insulin during the GTT (Fig. 4*I–K*). They also displayed abnormal pyruvate tolerance, suggesting altered hepatic gluconeogenesis (Fig. 4*L*). Consistent with the insulin tolerance test results, MI4KO mice fed the high-fat diet also had significantly higher fasting serum insulin levels, without a change in baseline glycemia (Fig. 4*M* and *N*).

Systemic insulin resistance in MI4KO mice is associated with increased inflammation. Because IRF4 acts as a suppressor of inflammation, we hypothesized that MI4KO mice would have increased DIO-induced inflammation in insulin-sensitive tissues. We looked first at white adipose tissue (WAT), which is typically infiltrated by macrophages after the onset of obesity that distribute in a heterogeneous pattern called "crown-like structures. Staining for the macrophage-specific marker F4/80 (encoded by *Emr1*) in the epididymal WAT of high-fat fed mice showed increased numbers of crown-like structures in MI4KO mice (Fig. 5*A* and *B*). Consistent with the immunohistochemistry data, QPCR analysis revealed that the expression of *Emr1* and genes related to M1 macrophage activation (*Nos2*, *Mif*, and *Tnfa*) was increased in the WAT of MI4KO animals (Fig. 5*C*). There was no obvious difference in hepatic lipid content between $Irf4^{flox/flox}$ and MI4KO mice (Fig. 5*D*); however, the expression of several inflammatory genes (*Ccl2q*, *Ccr2*, *Il1b*, *Il6*, and *Tnfa*) in liver was increased (Fig. 5*E*) and the expression of Emr1 was also elevated, suggesting increased macrophage infiltration in this tissue as well. In skeletal muscle, the expression of *Emr1* and inflammatory genes (*Ccl2* and *Tnfa*) was also increased (Fig. 5*F*).

We next examined whether this alteration in the inflammatory status of liver, skeletal muscle, and WAT causes changes in local insulin action. In liver, skeletal muscle, and WAT of MI4KO mice, insulin-dependent Akt phosphorylation was significantly reduced (Fig. 5*G*). Consistent

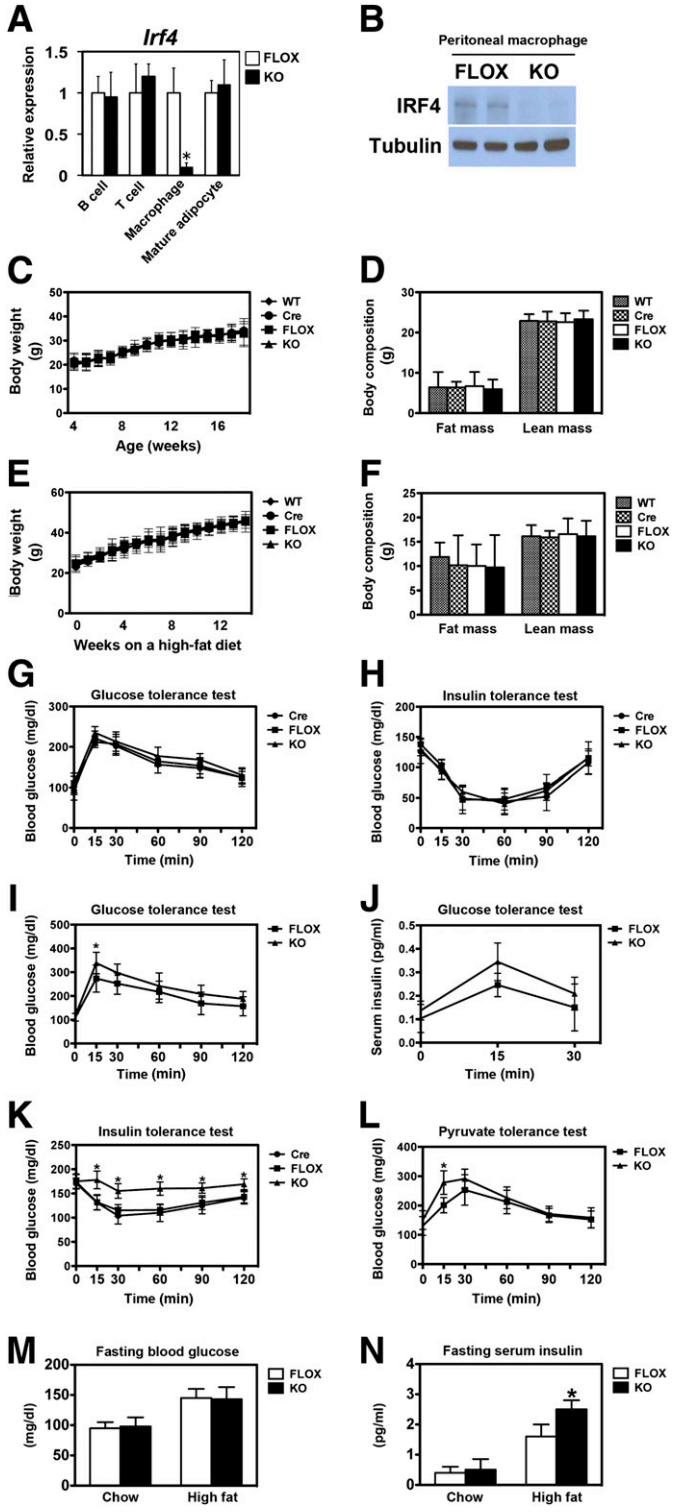

FIG. 4. Characterization of MI4KO (KO) mice compared with control *Irf4*$^{flox/flox}$ (FLOX) mice. *A*: *Irf4* mRNA expression in B cells, T cells, macrophages, and mature adipocytes of male control FLOX and KO mice (n = 3). Data are normalized to *Gapdh*. Results are expressed as mean ± SD. *P < 0.05 relative to FLOX mice. *B*: IRF4 protein expression in peritoneal macrophages of male FLOX and KO mice. *C*: Body weights of male WT, LysM-Cre (Cre), FLOX, and KO mice on chow diet (n = 10). Results are expressed as mean ± SD. *D*: Body composition analysis in 18-week-old male mice by MRI (n = 10). Results are expressed as mean ± SD. *E*: Body weights of male WT, Cre, FLOX, and KO mice on high-fat diet (n = 10). Results are expressed as mean ± SD. *F*: Body composition analysis by MRI in 18-week-old male mice fed the high-fat diet (n = 10). Results are expressed as mean ± SD. *G*: GTT on chow. Blood glucose in 18-week-old male Cre, FLOX, and KO mice fed the chow diet was determined at the indicated times after intraperitoneal injection with a bolus of glucose (n = 10). Results are expressed as mean ± SD. *H*: Insulin tolerance test on chow diet. Blood glucose in 20-week-old male Cre, FLOX, and KO mice fed the chow diet was determined at the indicated times after intraperitoneal injection with a bolus of insulin (n = 10). Results are expressed as mean ± SD. *I*: GTT on the high-fat diet. Blood glucose in 10-week-old male Cre, FLOX, and KO mice fed a high-fat diet was determined at the indicated times after intraperitoneal injection with a bolus of glucose (n = 7–8). Results are expressed as mean ± SD. *P < 0.05. *J*: Evoked insulin levels during the GTT shown in *I* (n = 7–8). Results are expressed as mean ± SD. *K*: Insulin tolerance test on high-fat diet. Blood glucose in 16-week-old male Cre, FLOX, and KO mice fed a high-fat diet was determined at the indicated times after intraperitoneal injection with a bolus of insulin (n = 10). Results are expressed as mean ± SD. *P < 0.05. *L*: Pyruvate tolerance test on high-fat diet. Blood glucose in 12-week-old male Cre, FLOX, and KO mice fed a high-fat diet was determined at the indicated times after intraperitoneal injection with a bolus of pyruvate (n = 7–8). Results are expressed as mean ± SD. *P < 0.05. *M*: Fasting glucose levels in chow and high-fat fed male mice (n = 10). Results are expressed as mean ± SD. *N*: Fasting insulin levels in chow and high-fat fed male mice (n = 10). Results are expressed as mean ± SD. *P < 0.05.

with the notion that increased local inflammation causes insulin resistance, we also noted enhanced activation of c-Jun N-terminal kinase (JNK) signaling in liver, skeletal muscle, and WAT of MI4KO mice (Fig. 5*H*). Taken together, these results suggest that IRF4 deficiency in macrophages is sufficient for the induction of inflammation and subsequent insulin resistance in multiple peripheral tissues.

Loss of IRF4 worsens the M1-to-M2 ATM imbalance in the context of high-fat feeding. We next investigated the status of ATM polarization in MI4KO and control mice. We isolated the SVF from epididymal fat pads excised from high-fat fed male MI4KO and control mice. The use of CD11c as a marker for M1 polarization and CD206 as a marker for M2 polarization in flow cytometry (30) demonstrated an increased M1-to-M2 ratio in MI4KO mice (Fig. 6*A*, Supplementary Fig. 1). We next measured mRNA expression of M1 and M2 markers in isolated ATMs by QPCR. The expression of M1 markers (*Ccl2*, *Il1b*, *Il6*, *Nos2*, and *Tnfa*) was significantly increased in MI4KO ATMs, whereas the expression of M2 markers (*Arg1*, *Chi3l3*, and *Mgl2*) was decreased in MI4KO ATMs (Fig. 6*B* and *C*). Finally, we sought to test the ability of *Irf4*$^{-/-}$ BMDMs to differentiate into M1 or M2 macrophages. GM-CSF can be used to induce M1 macrophage polarization in BMDMs, while M-CSF promotes M2 polarization (31–34). When treated with GM-CSF, *Irf4*$^{-/-}$ BMDMs expressed significantly higher amounts of *Il1b* and *Tnfa* than control BMDMs in response to palmitate. When treated with M-CSF, however, *Irf4*$^{-/-}$ BMDMs expressed significantly lower amounts of *Arg1* and *Chi3l3* than control BMDMs in response to IL-4 (Fig. 6*D*).

DISCUSSION

Macrophages play a significant role in the metabolic response to obesity, and understanding the transcriptional basis of macrophage polarization and function has become highly relevant to the quest for identifying new therapeutic targets for metabolic disease. We have been interested in the role of interferon regulatory factors generally, and IRF4 in particular, as transcriptional regulators of metabolism in adipocytes (16,17); our current data suggest that IRF4 plays an important metabolic role from within macrophages as well. IRF4 is induced in macrophages by

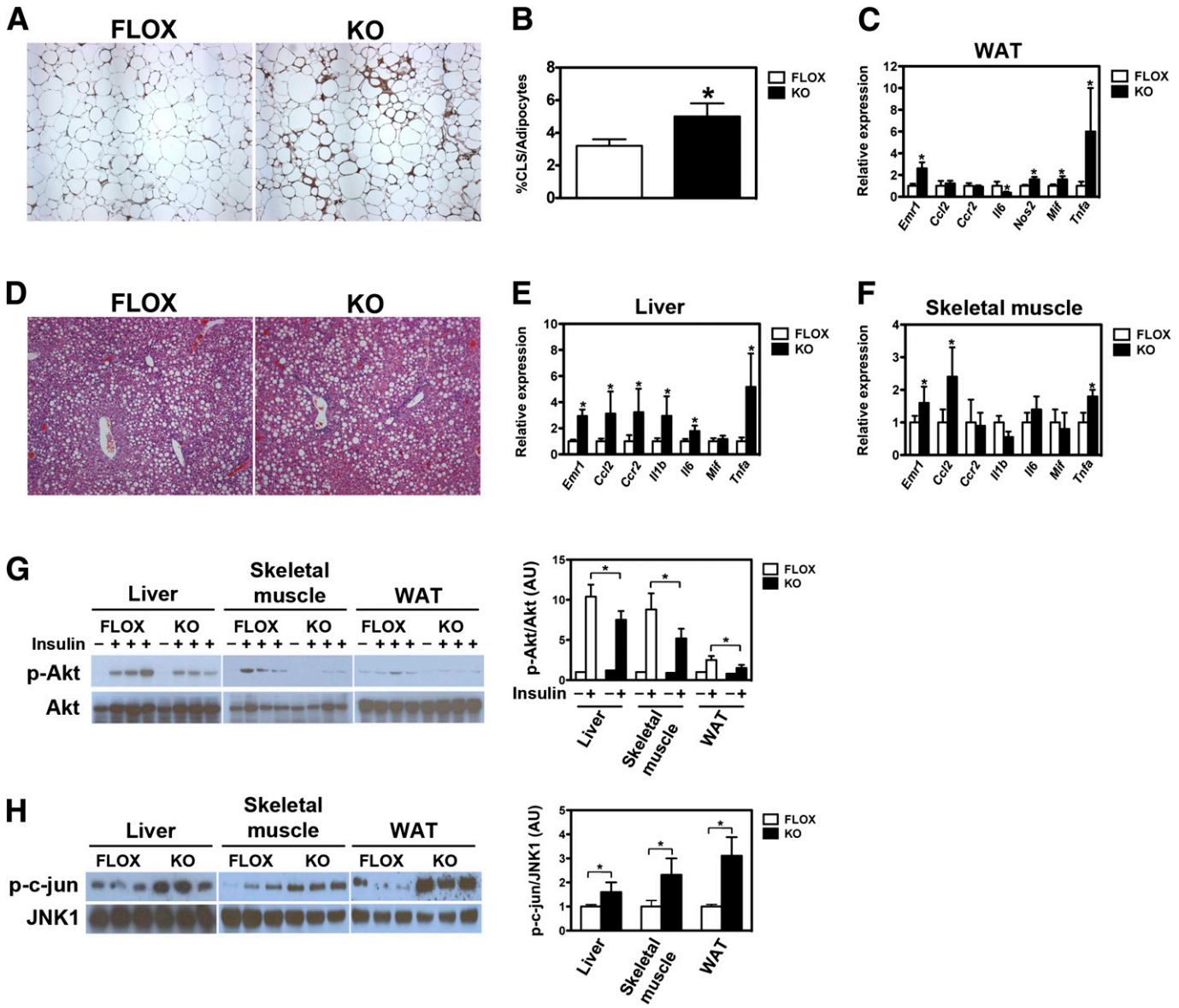

FIG. 5. Systemic insulin resistance in MI4KO (KO) mice compared with control *Irf4*$^{flox/flox}$ (FLOX) mice is associated with increased inflammation. *A*: Increased macrophage infiltration into WAT of KO mice as assessed by F4/80 staining. *B*: Quantification of F4/80-positive cells (n = 4 mice per group). *P < 0.05. *C*: QPCR analysis of genes related to inflammation in WAT (n = 7 mice per group). Data are normalized to *36B4* expression and are expressed as fold induction relative to FLOX. Results expressed as mean ± SD. *P < 0.05. *D*: Hematoxylin and eosin staining of liver. *E*: QPCR analysis of genes related to inflammation in liver (n = 7 mice per group). Data are normalized to *Gapdh* expression and are expressed as fold induction relative to FLOX. Results expressed as mean ± SD. *P < 0.05. *F*: QPCR analysis of genes related to inflammation in skeletal muscle (n = 7 mice per group). Data are normalized to *36B4* expression and are expressed as fold induction relative to FLOX. Results expressed as mean ± SD. *P < 0.05. *G*: Insulin-stimulated Akt phosphorylation (Ser473) in liver, skeletal muscle, and WAT of FLOX and KO mice. The graph to the *right* of the blots shows quantification. Data are shown as mean ± SD. *P < 0.05. *H*: In vitro phosphorylation of c-jun in liver, skeletal muscle, and WAT of FLOX and KO mice. The graph to the *right* of the blots shows quantification. Data are mean ± SD. *P < 0.05. AU, arbitrary units.

inflammatory (e.g., TLR4 ligands, LPS, and palmitate) and anti-inflammatory signals (e.g., IL-4), although in the former case, IRF4 appears to be activated as a "brake" on inflammatory gene expression. This is suggested by the fact that ablation of IRF4 from macrophages enhances inflammatory gene expression, and overexpression of IRF4 has the opposite effect. Consistent with these findings, *Irf4*$^{-/-}$ macrophages induce insulin resistance in cocultured adipocytes, and mice with a myeloid-specific deletion of IRF4 are insulin resistant without a change in adiposity.

Because polarization has such profound effects on cellular function and disease risk, the transcriptional pathways by which macrophages move along the spectrum between the M1 and M2 phenotypes has been the subject of intense inquiry. Multiple transcription factors have been shown to promote M2 polarization in particular, including STAT6 (1), PPARγ (8,9), PPARδ (10), and KLF4 (11). IRF4 was first proposed to regulate the inflammatory state of macrophages in 2005, when two groups published data showing that *Irf4*$^{-/-}$ macrophages display enhanced inflammatory cytokine expression, although the concept of polarization per se was not addressed (24,25). El Chartouni et al. (12) showed that IL-4 treatment, which induces M2 polarization, induces IRF4. Another recent study found the histone demethylase Jmjd3 was also induced by chitin,

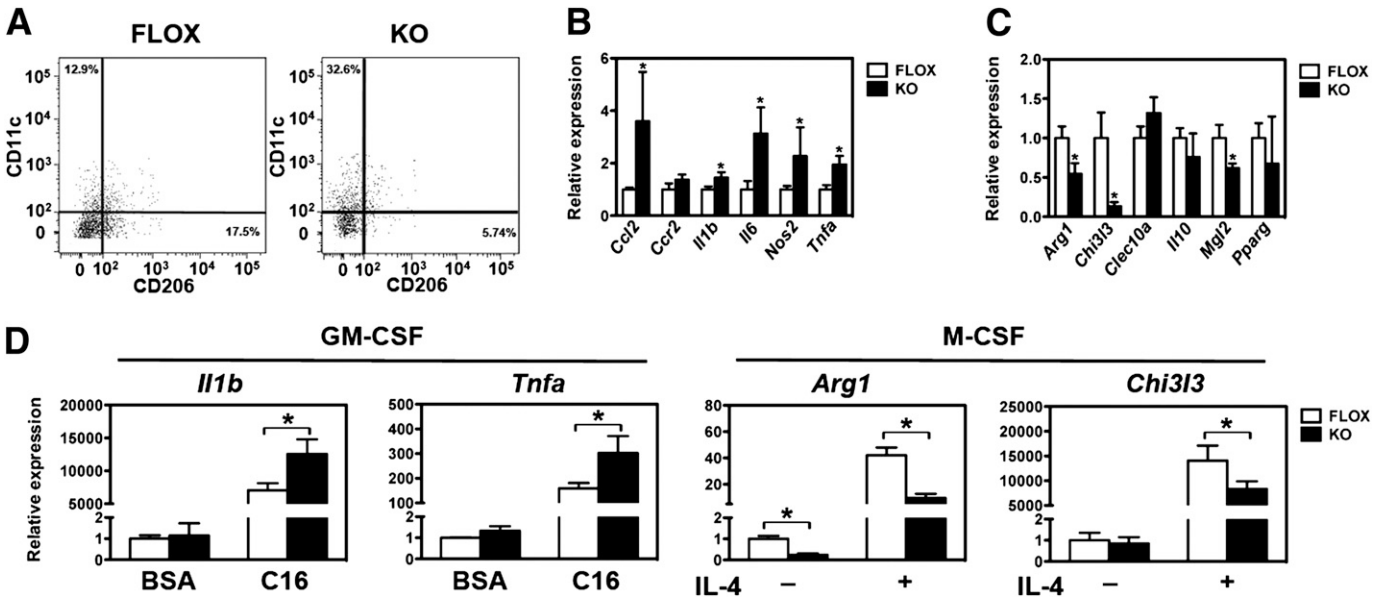

FIG. 6. IRF4 expression is associated with M2 ATM polarization in control *Irf4*$^{flox/flox}$ (FLOX) and MI4KO (KO) mice. *A*: SVF cells of epididymal adipose tissue were incubated with antibodies to CD11c and CD206 and analyzed using flow cytometry. *B*: mRNA expression of *Ccl2*, *Ccr2*, *Il1b*, *Il6*, *Nos2*, and *Tnfa* in ATMs (n = 5 mice per group). Data are expressed as mean ± SD. *$P < 0.05$. *C*: mRNA expression of *Arg1*, *Chi3l3*, *Clec10a*, *Il10*, *Mgl2*, and *Pparg* in ATMs (n = 5 mice per group). Data are expressed as mean ± SD. *$P < 0.05$. *D*: mRNA expression of *Il1b* and *Tnfa* in GM-CSF (50 ng/mL)-induced M1 BMDMs and M-CSF (50 ng/mL)-induced M2 BMDMs. QPCR analysis of *Il1b* and *Tnfa* levels after 16-h stimulation with BSA, 200 μmol/L palmitate (C16), or IL-4 (10 ng/mL). Data are normalized to *Gapdh* expression and expressed as fold induction relative to BSA. Results expressed as mean ± SD (n = 5). *$P < 0.05$.

a structural component of helminths and a known inducer of the M2 phenotype (13). *Jmjd3*$^{-/-}$ mice were shown to be susceptible to parasitic infection, in part because of deficient numbers of M2 macrophages. Among the genes whose expression was affected by the loss of Jmjd3 was *Irf4*, which was subsequently shown to mediate some of the effects on M2 polarization (13). Our work extends these findings by showing that resident ATMs require IRF4 to maintain their position on the polarization spectrum and by demonstrating that the M1-to-M2 imbalance that accompanies obesity is made worse in the absence of IRF4. Most importantly, we show that the lack of IRF4 in myeloid cells has profound consequences on insulin sensitivity in vitro and in vivo.

In brown and white adipocytes, we showed that IRF4 expression was highly responsive to nutritional state, such that fasting induced a huge increase in IRF4 mRNA and protein levels (17). This effect is mediated by FoxO1, which resides in the nucleus in the absence of insulin (as occurs in fasting). After feeding, rising levels of insulin promote the Akt-mediated phosphorylation and subsequent nuclear exclusion of FoxO1; this leads to sharp reductions in *Irf4* mRNA levels within hours. Could FoxO1 play a role in IRF4 expression in macrophages? It is possible, but the notion is contradicted by recent data from Kawano et al. (35), in which myeloid-specific knockout of Pdk1 (an upstream kinase of FoxO1) caused increased M1 polarization in adipose tissue with associated insulin resistance. This effect was phenocopied by myeloid-specific transgenic overexpression of a constitutively active FoxO1 and rescued by a dominant negative FoxO1 allele. Similarly, FoxO1 has been shown to promote TLR4 expression and inflammatory activation of macrophages (36). Although an effect on IRF4 per se was not assessed in either of these studies, the results are inconsistent with the idea that FoxO1 could be a major inducer of IRF4 and the M2 polarization program in macrophages.

We found that IL-4, a classic promoter of the M2 phenotype, does induce expression of IRF4 in PMs and BMDMs. The latter confirms the prior result of El Chartouni et al. (12), who proposed that STAT6 might be a transcriptional mediator of IL-4 on the IRF4 promoter; IL-4 *does* induce IRF4 through STAT6 in T helper lymphocytes (37), suggesting this may also be true in macrophages. The ability of LPS, acting through TLR4, to induce IRF4 is more puzzling, given its association with the induction of inflammatory cytokine expression. We demonstrate that palmitate, a nutritional fatty acid and proposed TLR4 ligand (18), has the same effect as LPS. The induction of IRF4 by TLR4 ligation is likely a "braking" or compensatory effect, because loss of IRF4 potentiates the ability of LPS and palmitate to induce inflammatory gene expression (13,24,25).

IRF4 is a transcription factor with a functional DNA binding domain and is known to bind to specific promoter sequences in macrophages, sometimes in concert with other factors like PU.1 (38). Interestingly, IRF4 can also be localized to the cytosol (25,38), where it has been shown to bind to MyD88, a critical downstream factor in the TLR4-driven innate immune response. In this context, IRF4 has been proposed to compete with the proinflammatory IRF5 for binding to MyD88, setting up a scenario in which IRF4 exerts at least some its anti-inflammatory activity in a way that does not require nuclear localization or DNA binding. We do not know the extent to which this nongenomic activity could contribute to the metabolic consequences of IRF4 deletion in macrophages. Furthermore, there is as yet no evidence for such nongenomic action in any IRF4-expressing cell type other than macrophages, despite the presence of TLR4, MyD88, and IRF5 in adipocytes, for example. To address this issue, we are developing new models of transgenic IRF4 expression in which WT or DNA binding domain mutant alleles can be expressed in a tissue-selective fashion.

Taken together, our data suggest that IRF4 exerts actions on metabolic physiology from at least two cell types, the adipocyte and the macrophage. In adipocytes, IRF4 promotes lipolysis and represses lipogenesis in a nutritionally regulated fashion. Mice lacking IRF4 specifically in adipose tissue have enhanced weight gain and are insulin resistant. IRF4 in macrophages represses innate immunity, and mice lacking IRF4 specifically in myeloid cells show reduced insulin sensitivity, even in the absence of changes in adiposity. Evolutionarily, IRFs are an ancient family, having evolved in concert with the development of multicellularity; identifiable IRF4 precursors are among the very earliest isoforms noted (39). Multicellularity requires cells to take on specialized roles, such as energy acquisition and storage or host defense. A theme in evolution is the co-option of molecules for disparate roles in different tissues, and IRF4 appears to be no exception. What we have learned over the past decade or so is that important metabolic cross talk occurs between cell types and organs, including immune cells previously not suspected of participating in systemic nutrient homeostasis. IRF4 represents a key node in this cross talk by regulating multiple aspects of the physiological response to nutrients and obesity in different tissues.

ACKNOWLEDGMENTS

This work was funded by a research grant from the Astellas Foundation for Research on Metabolic Disorders, Suzuken Memorial Foundation, Mochida Memorial Foundation for Medical and Pharmaceutical Research, The Okayama Medical Foundation, Takeda Science Foundation, Yamaguchi Endocrine Research Foundation, and Japan Society for the Promotion of Science (to J.E.), and National Institutes of Health R01-DK-63906 and R01-DK-085171 (to E.D.R.).

No potential conflicts of interest relevant to this article were reported.

J.E., X.K., and E.D.R. determined the experimental plan. J.E., X.K., M.T., X.W., and S.K. did the experiments. J.E. and E.D.R. analyzed the data and wrote the manuscript. E.D.R. is the guarantor of this work, and, as such, had full access to all the data in the study and takes responsibility for the integrity of the data and the accuracy of the data analysis.

The authors thank Drs. Kunihiko Ichinose (Nagasaki University Graduate School of Biomedical Sciences), Tetsuya Hosooka (Kobe University Graduate School of Medicine), and Choel Son (Kyoto University Graduate School of Medicine) for technical advice, and members of the Rosen laboratory (BIDMC) for helpful discussion. Ulf Klein at Columbia University provided *Irf4*$^{flox/flox}$ mice.

REFERENCES

1. Gordon S. Alternative activation of macrophages. Nat Rev Immunol 2003;3:23–35
2. Olefsky JM, Glass CK. Macrophages, inflammation, and insulin resistance. Annu Rev Physiol 2010;72:219–246
3. Sica A, Mantovani A. Macrophage plasticity and polarization: in vivo veritas. J Clin Invest 2012;122:787–795
4. Lumeng CN, Bodzin JL, Saltiel AR. Obesity induces a phenotypic switch in adipose tissue macrophage polarization. J Clin Invest 2007;117:175–184
5. Lumeng CN, Deyoung SM, Bodzin JL, Saltiel AR. Increased inflammatory properties of adipose tissue macrophages recruited during diet-induced obesity. Diabetes 2007;56:16–23
6. Fujisaka S, Usui I, Bukhari A, et al. Regulatory mechanisms for adipose tissue M1 and M2 macrophages in diet-induced obese mice. Diabetes 2009;58:2574–2582
7. Patsouris D, Li PP, Thapar D, Chapman J, Olefsky JM, Neels JG. Ablation of CD11c-positive cells normalizes insulin sensitivity in obese insulin resistant animals. Cell Metab 2008;8:301–309
8. Odegaard JI, Ricardo-Gonzalez RR, Goforth MH, et al. Macrophage-specific PPARgamma controls alternative activation and improves insulin resistance. Nature 2007;447:1116–1120
9. Bouhlel MA, Derudas B, Rigamonti E, et al. PPARgamma activation primes human monocytes into alternative M2 macrophages with anti-inflammatory properties. Cell Metab 2007;6:137–143
10. Kang K, Reilly SM, Karabacak V, et al. Adipocyte-derived Th2 cytokines and myeloid PPARdelta regulate macrophage polarization and insulin sensitivity. Cell Metab 2008;7:485–495
11. Liao X, Sharma N, Kapadia F, et al. Krüppel-like factor 4 regulates macrophage polarization. J Clin Invest 2011;121:2736–2749
12. El Chartouni C, Schwarzfischer L, Rehli M. Interleukin-4 induced interferon regulatory factor (Irf) 4 participates in the regulation of alternative macrophage priming. Immunobiology 2010;215:821–825
13. Satoh T, Takeuchi O, Vandenbon A, et al. The Jmjd3-Irf4 axis regulates M2 macrophage polarization and host responses against helminth infection. Nat Immunol 2010;11:936–944
14. Chaudhuri AA, So AY, Sinha N, et al. MicroRNA-125b potentiates macrophage activation. J Immunol 2011;187:5062–5068
15. Lech M, Weidenbusch M, Kulkarni OP, et al. IRF4 deficiency abrogates lupus nephritis despite enhancing systemic cytokine production. J Am Soc Nephrol 2011;22:1443–1452
16. Eguchi J, Yan QW, Schones DE, et al. Interferon regulatory factors are transcriptional regulators of adipogenesis. Cell Metab 2008;7:86–94
17. Eguchi J, Wang X, Yu S, et al. Transcriptional control of adipose lipid handling by IRF4. Cell Metab 2011;13:249–259
18. Shi H, Kokoeva MV, Inouye K, Tzameli I, Yin H, Flier JS. TLR4 links innate immunity and fatty acid-induced insulin resistance. J Clin Invest 2006;116:3015–3025
19. Furuhashi M, Fucho R, Görgün CZ, Tuncman G, Cao H, Hotamisligil GS. Adipocyte/macrophage fatty acid-binding proteins contribute to metabolic deterioration through actions in both macrophages and adipocytes in mice. J Clin Invest 2008;118:2640–2650
20. Lumeng CN, Deyoung SM, Saltiel AR. Macrophages block insulin action in adipocytes by altering expression of signaling and glucose transport proteins. Am J Physiol Endocrinol Metab 2007;292:E166–E174
21. Klein U, Casola S, Cattoretti G, et al. Transcription factor IRF4 controls plasma cell differentiation and class-switch recombination. Nat Immunol 2006;7:773–782
22. Joost HG, Schürmann A. Subcellular fractionation of adipocytes and 3T3-L1 cells. Methods Mol Biol 2001;155:77–82
23. Osborn O, Olefsky JM. The cellular and signaling networks linking the immune system and metabolism in disease. Nat Med 2012;18:363–374
24. Honma K, Udono H, Kohno T, et al. Interferon regulatory factor 4 negatively regulates the production of proinflammatory cytokines by macrophages in response to LPS. Proc Natl Acad Sci U S A 2005;102:16001–16006
25. Negishi H, Ohba Y, Yanai H, et al. Negative regulation of Toll-like-receptor signaling by IRF-4. Proc Natl Acad Sci U S A 2005;102:15989–15994
26. Zuckerman SH, Evans GF, Guthrie L. Transcriptional and post-transcriptional mechanisms involved in the differential expression of LPS-induced IL-1 and TNF mRNA. Immunology 1991;73:460–465
27. Vallabhapurapu S, Karin M. Regulation and function of NF-kappaB transcription factors in the immune system. Annu Rev Immunol 2009;27:693–733
28. Matsuyama T, Grossman A, Mittrücker HW, et al. Molecular cloning of LSIRF, a lymphoid-specific member of the interferon regulatory factor family that binds the interferon-stimulated response element (ISRE). Nucleic Acids Res 1995;23:2127–2136
29. Yamagata T, Nishida J, Tanaka S, et al. A novel interferon regulatory factor family transcription factor, ICSAT/Pip/LSIRF, that negatively regulates the activity of interferon-regulated genes. Mol Cell Biol 1996;16:1283–1294
30. Tiemessen MM, Jagger AL, Evans HG, van Herwijnen MJ, John S, Taams LS. CD4+CD25+Foxp3+ regulatory T cells induce alternative activation of human monocytes/macrophages. Proc Natl Acad Sci U S A 2007;104:19446–19451
31. Fleetwood AJ, Lawrence T, Hamilton JA, Cook AD. Granulocyte-macrophage colony-stimulating factor (CSF) and macrophage CSF-dependent macrophage phenotypes display differences in cytokine profiles and transcription factor activities: implications for CSF blockade in inflammation. J Immunol 2007;178:5245–5252
32. Fleetwood AJ, Dinh H, Cook AD, Hertzog PJ, Hamilton JA. GM-CSF- and M-CSF-dependent macrophage phenotypes display differential dependence on type I interferon signaling. J Leukoc Biol 2009;86:411–421

33. Martinez FO, Gordon S, Locati M, Mantovani A. Transcriptional profiling of the human monocyte-to-macrophage differentiation and polarization: new molecules and patterns of gene expression. J Immunol 2006;177:7303–7311
34. Verreck FA, de Boer T, Langenberg DM, et al. Human IL-23-producing type 1 macrophages promote but IL-10-producing type 2 macrophages subvert immunity to (myco)bacteria. Proc Natl Acad Sci U S A 2004;101:4560–4565
35. Kawano Y, Nakae J, Watanabe N, et al. Loss of Pdk1-Foxo1 signaling in myeloid cells predisposes to adipose tissue inflammation and insulin resistance. Diabetes 2012;61:1935–1948
36. Fan W, Morinaga H, Kim JJ, et al. FoxO1 regulates Tlr4 inflammatory pathway signalling in macrophages. EMBO J 2010;29:4223–4236
37. Goswami R, Jabeen R, Yagi R, et al. STAT6-dependent regulation of Th9 development. J Immunol 2012;188:968–975
38. Marecki S, Atchison ML, Fenton MJ. Differential expression and distinct functions of IFN regulatory factor 4 and IFN consensus sequence binding protein in macrophages. J Immunol 1999;163:2713–2722
39. Nehyba J, Hrdlicková R, Bose HR. Dynamic evolution of immune system regulators: the history of the interferon regulatory factor family. Mol Biol Evol 2009;26:2539–2550